Journal of Materials Chemistry C

Strain-Controlled Optical Transmittance Tuning of Three-Dimensional Carbon Nanotube Architectures

Journal:	*Journal of Materials Chemistry C*
Manuscript ID	TC-ART-11-2018-005747.R1
Article Type:	Paper
Date Submitted by the Author:	16-Jan-2019
Complete List of Authors:	Li, Yang; Nanjing University of Aeronautics and Astronautics Owuor, Peter; Rice University Dai, Zhendong; Nanjing University of Aeronautics and Astronautics, Xu, Quan; China University of Petroleum (Beijing), Institute of New Energy Rodrigo, Villegas; Rice University Kishore, Sharan; Indian Institute of Science, Materials Engineering Vajtai, Robert; Rice University, Tour, James; Rice University, Chemistry Dept and NanoCarbon Center Lou, Jun; Rice University, Department of Materials Science and NanoEngineering Tiwary, Chandra; Rice University, Materials Science and NanoEngineering Ajayan, Pulickel; Rice University, Department of Mechanical Engineering & Materials Science

Journal of Materials Chemistry C

ARTICLE

Strain-Controlled Optical Transmittance Tuning of Three-Dimensional Carbon Nanotube Architectures

Received 00th January 20xx,
Accepted 00th January 20xx

DOI: 10.1039/x0xx00000x

www.rsc.org/

Yang Li,[a,b,+] Peter Samora Owuor,[b,+] Zhendong Dai,[a*] Quan Xu,[c*] Rodrigo V. Salvatierra,[b] Sharan Kishore,[d] Robert Vajtai,[b] James M. Tour,[b] Jun Lou,[b] Chandra Sekhar Tiwary,[b,e*] Pulickel M. Ajayan[b]

Three-dimensional (3D) architectures based on carbon nanotubes (CNTs) have been applied to fields ranging from aerospace to biomedicine. In this report, the fabrication of 3D CNT patterns having various orientations has been described. These 3D architectures acted both as efficient optical switching devices and barriers to protect against laser-induced damage. Such devices can switch from transparent to opaque upon application of a very small strain (<0.4%). Optical switching depends heavily on the orientations of the anisotropic patterns. The orientation dependence of 3D CNT architecture mechanical properties was also studied experimentally and further supported by finite element method analysis.

Introduction

Anisotropy is found in most natural composites such as wood, bone,[1] seashells,[2] and so on. Nature selects smart natural composite structures such that their Young's moduli, fluid flow characteristics, and other functional properties are anisotropic. This has led to bio-inspired designs such as an optical switching material whose optical properties like color and transmittance can be tuned by mechanical,[3,4] electrical,[5-13] and chemical stimuli,[14] and so on.[15-17] Several biomimetic structures made from carbon nanotubes (CNTs) have recently been reported to have unique mechanical,[18-22] adhesive,[23,24] and other properties. Three-dimensional (3D) CNTs, which have a refractive index of 2.5 and an absorption coefficient of less than 1, can be considered the darkest known materials.[25,26] In addition, their superior elasticity allows the CNT to accommodate large strain deformations without structural failure.[27,28] When vertically grown in a forest-like arrangement with good alignment, CNTs form an extremely resilient structure where individual nanotubes act like nanoscale struts.[27] A well-designed CNT structure can exhibit anisotropy in either its mechanical or optical properties, especially when combined with polymers such as polydimethylsiloxane (PDMS). Such a composite simultaneously exhibits the stiffness of CNTs and elasticity of PDMS. Reinforcing the CNT structures with polymers also results in several interesting properties such as self-stiffening[21] and strain hardening.[29] Researchers have been able to combine the mechanical and optical properties of 3D CNTs and design mechano-optical switching structures.[30,31] Mechanical modulation has been widely used to control optical light transmission in buildings via various means such as smart windows, which can switch from opaque to transparent to save energy.[31] However, these approaches are plagued with problems such as inefficiency and high strain; thus, they require a great deal of advancement before they can truly be the "smart" windows of the future. Owing to the sophistication required to realize current smart windows, there is a need for a simpler strategy that offers better alternatives with lower strain. Furthermore, as lasers have become more prevalent in biomedical, optical components, and advanced engineering technologies, laser-induced damage in these areas has received increasing attention.[32-34] Thus, designing convenient and effective laser-shielding materials has become increasingly important.

In this study, we report a CNT/PDMS composite structure with tunable optical transmittance, i.e., the ability to transition from transparent to opaque in response to a strain of less than 0.4%, which is the most sensitive value achieved to date to the best of our knowledge. CNT patterns were designed as straight, corner-shaped, and curved stripes, as well as pillars. The geometries of the 3D CNT architectures and the inherent anisotropic mechanical properties were used to control the corresponding mechanical responses. In

[a] *Institute of Bio-inspired Structure and Surface Engineering, Jiangsu Provincial Key Laboratory of Bionic Functional Materials, College of Astronautics, Nanjing University of Aeronautics & Astronautics, Nanjing 210016, China Email: zddai@nuaa.edu.cn*

[b] *Department of Materials Science and NanoEngineering, Department of Chemistry, Rice University, Houston, Texas, 77005, USA Email: cst.iisc@gmail.com*

[c] *State Key Laboratory of Heavy Oil Processing, China University of Petroleum-Beijing, 102249, China Email: xuquan@cup.edu.cn*

[d] *Department of Mechanical Engineering, Arizona State University, Arizona, 85287, USA*

e. Metallurgical and materials engineering, Indian Institute of Technology Kharagpur, West bengal-721302, India

[+] These authors contributed equally.

† Electronic Supplementary Information (ESI) available: Fig. S1–S9. See DOI: 10.1039/x0xx00000x

addition, the transition from transparent to opaque depended heavily on the orientations of the anisotropic patterns. Moreover, such structures could also block laser irradiation. Finally, we also analyzed the mechanical behaviors of various CNT patterns using the finite element method (FEM). The simplicity of our approach shows the advantages of such materials, which can be employed as both effective optical switches and barriers to protect against laser-induced damage.

Materials and methods

Pattern preparation. As shown in Figure 1a, conventional photolithography, electron beam catalyst deposition, and thermal chemical vapor deposition (CVD) were used to fabricate patterned, vertically aligned CNTs with four different geometries.

In the first step, photolithography was used to design patterns with various morphologies on silicon wafers. Pre-patterned chrome masks with certain geometric parameters (including pillars and curved, corner-shaped, and straight structures) were fabricated. During photolithography, a positive photoresist (AZ5214) was coated on top of the Si/SiO_2 wafer. The photoresist was selectively exposed through a chrome mask under 365 nm UV light in a clean room. The exposed photoresist was then removed through developing. Typical CNT growth catalyst layers (20 nm thick Al_2O_3 layer and 2 nm thick Fe film) were successively deposited on the patterned Si/SiO_2 substrate using an electron beam system (E-beam 500, Xingnan). Before CVD growth, the catalyst-coated un-exposed photoresist was etched away via immersion in acetone for 10 min, leaving behind the selected patterns. Thus, the catalyst was deposited on the photoresist-free area, as shown in the electronic supplementary information (ESI) Figure S1.

CNTs were grown in a tubular furnace (OTF-1200X-80, Kejing) via thermal CVD with 1200 sccm of Ar used as the carrier gas. At 650 °C, 450 sccm of H_2 was injected into the furnace to pretreat the catalyst. CNTs were precipitated when 250 sccm C_2H_2 was introduced into the reactor at 720 °C. The reaction durations were in the range of 3–30 min, and the CNT lengths varied from 100 to 800 μm. When growth was complete, the C_2H_2 and H_2 flows were stopped, but the Ar flow was continued until the samples reached a temperature of 25 °C.

Commercially available PDMS (Sylgard 184, Dow Corning) was prepared by mixing 10 mL of the monomer with 2 mL of the curing agent in a vial. We selected PDMS because of its transparency and elasticity. PDMS was infiltrated into the patterned CNTs in a culture dish that was then placed in an oven at 65 °C for 5 h until PDMS was completely cured. Then, the cured sample was directly taken out of the culture dish. Excess PDMS was cut along the PDMS/CNT edge.

Laser experiments were conducted with a model XLS10MWH (Universal Laser System) laser cutter using a 1.06 μm laser at 30 kHz and a 30% duty cycle (100% power = 50 W). The laser was set to scribe a circle of 0.5 cm diameter at a rate of 15.24 cm s^{-1}, with an image density of 500 pulses per inch. The sample dimensions were 11 × 7 × 4 mm. For SEM analysis, the PDMS samples were carefully cut with a blade to expose the burnt area.

Optical measurements. A goniometer was used to observe the transitions between transparency and opacity. Samples were strained, the transmitted light was observed, and optical images were taken.

Dynamic mechanical testing. Samples were loaded in the compression mode for an isothermal test. The stiffness was monitored along with the number of loading cycles. All tests were conducted on a dynamic analysis instrument (Q800 DMA). The frequency was maintained at 1 Hz in order to allow cyclic compressive loading while eliminating the risks of resonant or inertial effects.

Simulation details. A solid model comprising alternating layers of PDMS and CNTs was constructed using SolidWorks. A total of three models were constructed with various PDMS and CNT geometries. Static structural simulations were performed on the three models using ANSYS Workbench. CNTs were modelled as isotropic materials with Young's moduli and Poisson's ratios of 300 MPa and 0 respectively, while the PDMS was modelled as a neo-Hookean hyper-elastic material. The neo-Hookean constants D1 and C10 were calculated using the bulk and shear moduli, respectively. Bonded contacts were established between the layers. The three models exhibited different behaviors upon the application of uniaxial pressure in various directions. To analyze these stress distribution patterns, a design of experiments (DOE) comprised of nine iterations (three models and three directions of pressure) was created and simulated. A pressure of 0.1 MPa was applied to the required face and maintained for all iterations. The face parallel to the surface that received the load was always defined as a fixed support. This arrangement is similar to that of a uniaxial compression test. The large deformation option was turned "on" to detect the geometric and material non-linear behavior. Plots of von Mises stress, elastic strain, and total deformation were generated, and their respective scales were kept constant for all iterations of the DOE.

RESULTS AND DISCUSSION

Figure 1b shows the various types of fabricated patterns. In straight stripe patterns, the vertically aligned CNTs were embedded inside the polymer matrix along the thickness direction of the composite block. The main difference between the curved and corner-shaped stripe patterns was the smoothness of the curve. The measured misalignment angle for the corner-shaped stripe pattern was 134°, compared to 165° for the curved stripe. The pillars were fabricated onto the micro- or nano-circular patterns created on the silicon wafer. This photolithography technique produced hundreds of thousands of CNTs on one circular pattern (**ESI Figure S2**). A catalyst layer without patterns was

created on the silicon wafer to form arrays. The catalyst layer was deposited directly on substrate, and the vertically aligned CNTs grew into forest-like bundles. However, the vertically aligned structure of CNT array shrank and aggregated when it was infiltrated with PDMS (**ESI Figure S3**), which might have been due to the closely packed structure and the effect of capillary forces.[35] Therefore, a control sample with short CNT powder dispersed in the polymer matrix as conventional, randomly aligned CNT nanocomposites was fabricated, hereafter referred to as the "powder pattern" (**ESI Figure S4**). As shown in Figure 1c, optical images clearly identified the CNT-containing black regions. The CNT regions did not transmit light under optical illumination (**ESI Figure S5**) and thus created a contrast with the PDMS-rich regions. Low-magnification SEM images further demonstrated the previously discussed distinctive patterns (Figure 1c).

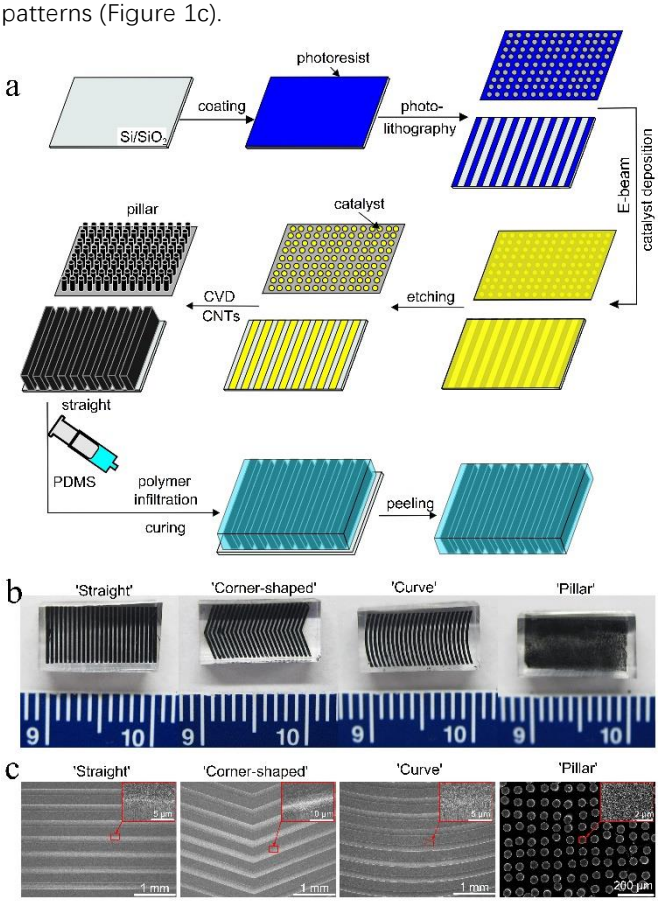

Fig. 1. Fabrication of patterned carbon nanotubes/PDMS composites. (a) Schematic representation of the patterned CNT/PDMS structure. The method combines photolithography, chemical vapor deposition, and polymer infiltration; (b) Optical images of the patterned CNT/PDMS composite. Pillars were made via circular etching, which left a circular catalyst region upon which the CNTs were grown. Straight, curved, and corner-shaped stripes in the lower panel are all defined by their catalyst patterns after lithography; (c) Low-magnification SEM images showing the distinct contours of patterned CNT forests. High-magnification SEM image (inset) of a pattern showing clear CNT forests with minimal buckling. Pillar patterns contained rod-like structures composed of CNT bundles.

High-magnification SEM images (inset, Figure 1c) revealed vertically aligned, uniformly distributed CNT forests in all patterns. This observation demonstrated that straight CNT forests with minimal buckling and entanglement could be grown. The integrities of the pillar patterns were maintained, in contrast with the powder pattern samples, which consisted of typical networked CNT bundle structures (**ESI Figure S4**). In most strain-controlled optical switching studies, "complete" switching between opacity and transparency is achieved with strain values greater than 1%.[3,36] The results of our patterned CNT/PDMS composite structure showed that this switching can be achieved using a much smaller strain (< 0.4%) and that such a composite structure is quite flexible. Optical transmittance changes were measured by straining the samples perpendicularly and longitudinally to the CNT patterns. The switch from transparent to opaque was found to be orientation-dependent. For a straight pattern, a plot of strain versus light intensity showed that the maximum opacity was achieved when the load was perpendicular to the direction of the CNTs (Figure 2a). The intensity changed from a normalized value of 1 with an unloaded sample to ~0.2 at a strain of 0.35% (Figure 2b and inset images). However, longitudinal loading of the straight pattern did not achieve the same result at the same strain (**ESI Figure S6**). Similar results were observed with the "curved stripe" pattern, where perpendicular loading led to a complete transition from transparent to opaque (intensity change from 1 to <0.2) at the same strain values. Longitudinal loading again did not show any meaningful transition to opacity at the same strain (**ESI Figure S7**). On the other hand, the transition to opacity (from 1 to <0.1) occurred at a strain of less than 0.125% with the "corner-shaped stripe" pattern. Longitudinal loading of the "corner" pattern again produced a minimal change in opacity (**ESI Figure S8**). The pillars and powdered patterns did not change as they were initially opaque because of the proximity of the CNTs (Figure 2b and **ESI Figure S9**). Compared with the wrinkled PDMS sheets in references,[3,36] pre-stretching is not necessary to create various wrinkling patterns for patterned CNT/PDMS composite. In our work, CNT patterns have been assembled inside the PDMS sheet before the stain was applied. The anisotropic pattern structure with a narrow gap distance can help achieving the switching under a much smaller strain (< 0.4%). In addition, because of their highly anisotropic nanoscale filamentary structure and extraordinary light absorption property,[37,38] Carbon nanotubes can be applied for optical applications such as ultra-dark surfaces, which could beneficial for improving the light-preventing efficiency. This strain dependent transition from clear to opaque was used in a simple light-switching device. As shown in Figure 2c and d, light was transmitted when there was no strain or load but was blocked when the device was strained.

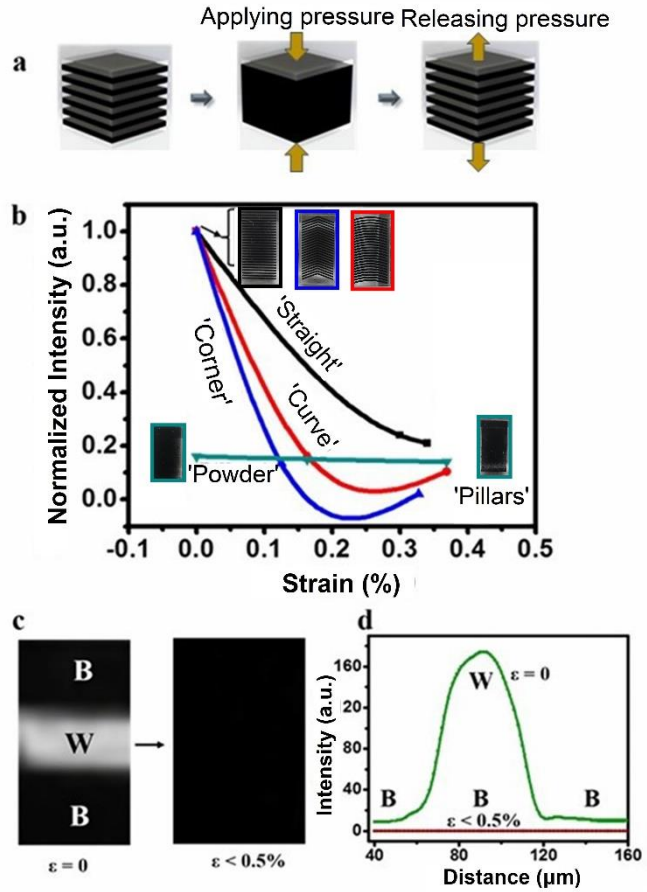

Fig. 2. Strain-controlled optical switching. (a) Schematic representation of the dependence of optical switching-on force. Application of perpendicular force or pressure produced a completely opaque structure; (b) Normalized intensity of transmitted light of all patterns (inset digital images). A decrease in perpendicular strain led to total opacity at a maximum strain of less than 0.4%. The powdered samples and "pillars" started at a much lower light intensity than the other patterns, and hence no changes could be observed; (c) Optical images showing changes between transparency (marked W) and opacity (marked B). (d) Plot of light intensity changes under different strain.

To elucidate the optical behaviors of various CNTs patterns/PDMS composite structure due to anisotropic loading, we quantified the pattern stiffness under dynamic loading. The stiffness tests were performed by subjecting the samples to constant loads and observing their responses under ambient conditions. Figure 3a shows the response of a sample patterned as a straight stripe. Analysis of the two loading configurations indicated that longitudinal loading produced more stiffness than perpendicular loading. Therefore, a smaller load was needed to compress the sample in the perpendicular direction of the patterns. This finding aligns well with the previous observation of the complete transition from clear to opaque under a very small strain. The same trend is observed with curved stripe patterns (Figure 3b). The longitudinally loaded samples were more than twice as stiff as the perpendicularly loaded samples. Again, this behavior occurred because the perpendicularly loaded samples required less strain to become opaque. The corner-shaped stripe patterns behaved in a similar manner, i.e., longitudinally loaded samples had higher stiffness

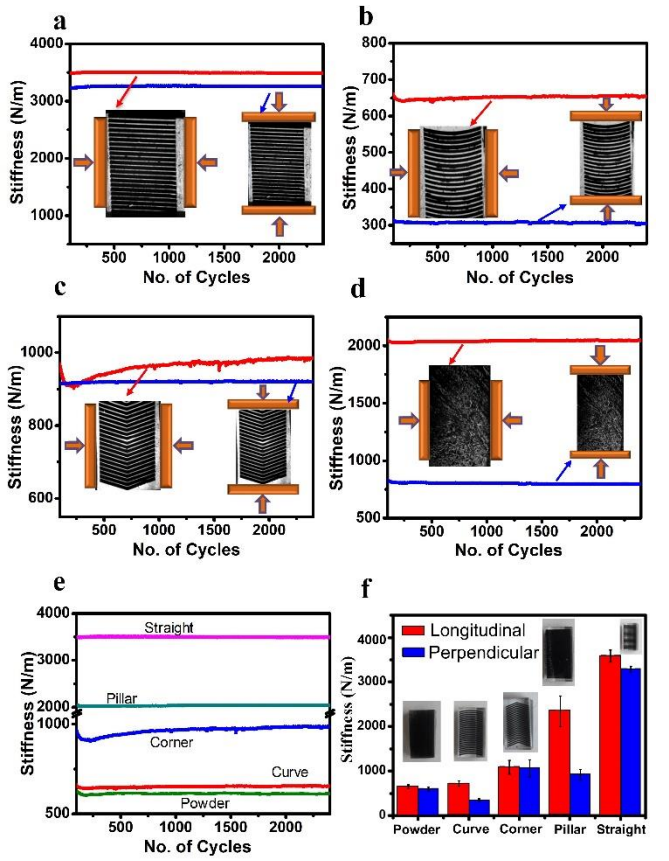

Fig. 3 Anisotropic mechanical responses. (a) Longitudinal and perpendicular mechanical responses of "straight" patterns. High stiffness was observed in the CNT loading direction (inset images); (b) The high stiffness of the "curved" pattern when loaded in a longitudinal direction differs from the results of perpendicular loading. The former produced almost twice the stiffness of the latter; (c) Longitudinally loaded "corner" pattern with high stiffness; (d) The stiffness of the longitudinally loaded pillars increased by 2.5×; (e, f) Comparing the patterns indicated high stiffness with the straight pattern and the lowest stiffness with the powder pattern, regardless of loading direction.

(Figure 3c). Further observation of the two curves in Figure 3c showed that the stiffness was almost identical during the initial cycle of loading. The stiffness of the longitudinally loaded sample increased linearly with the number of loading cycles. With the pillars, we also observed high stiffness of longitudinally loaded samples (Figure 3d). Overall, the straight stripe patterns exhibited the highest stiffness, while the conventional CNT dispersion, referred to as the "powder", had the lowest stiffness (Figure 3e and f) regardless of the direction of loading.

The pattern stiffness may vary because of the difference in CNT lengths. For instance, CNTs in the straight stripe patterns may form continuous, parallel, fiber-like bundles that produce a rigid structure.[27,39] Loads can be transferred

smoothly as a result of continuity in the bundles. When these bundles are aggregated in the polymer matrix, they resist large, longitudinal forces, but bend in response to perpendicular loading. The same load transfer mechanism occurs in the pillar pattern, but with less stiffness owing to the short CNTs.

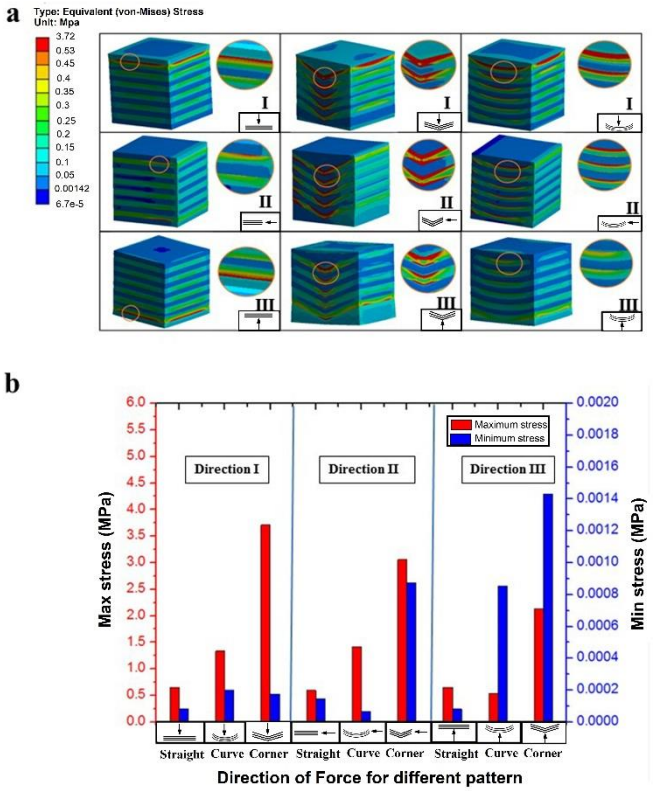

Fig. 4 Finite element analyses of CNT patterns. (a) Stress distributions of CNT patterns (straight, corner-shaped, and curved) indicating that better stress distributions within the straight patterns lead to a high stiffness. Stress concentration regions result from the corner-shaped pattern, especially at the interface between CNT forests and PDMS. The curved pattern eliminated the stress concentration regions; (b) Maximum and minimum stresses associated with all loading directions for all patterns.

FEM analysis was used to understand and explain the varying mechanical responses of the CNT patterns. The FEM was used to simulate the impacts of various loading criteria on CNT patterns in PDMS. We simulated the straight, corner-shaped, and curved stripe patterns. As shown in Figure 4a, the patterns experienced a load in the perpendicular (I), longitudinal (II), and perpendicular applicate (III) directions. The maximum and minimum stresses of the straight striped patterns appeared to be similar, which indicated better load transfer, especially under longitudinal loading. CNT forests easily transferred their loads in this configuration, resulting in very stiff structures. The corner-shaped stripe patterns behaved differently from the straight patterns, as the corners concentrated stress. Stress concentration was observed in all loading directions (I, II, and III) and resulted in structures with damping characteristics, as indicated by their large maximum and minimum stresses (Figure 4b). This was consistent with our experimental observations. The curved patterns exhibited high maximum stresses in loading directions I and II, but perpendicular loading from below produced very low maximum and minimum stresses. The curved architecture produced a better stress distribution by eliminating the stress concentration regions within the patterns. The maximum and minimum stresses that the various structures produced in response to loads from each direction are shown in Figure 4b. For directions I and II, the stress

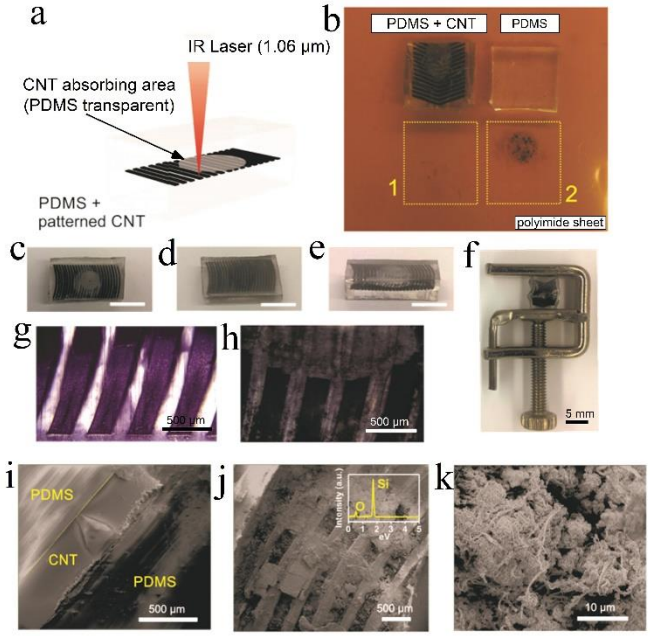

Fig. 5 Laser shield application. (a) Patterned CNTs block the 1.06 μm laser; (b) Photograph shows the effect of the laser shield experiment on a polyimide (PI) sheet. Pure PDMS (top right) was transparent to the 1.06 um laser, thus the laser burned the PI layer. The square at bottom right (square 2) indicates the location of the pure PDMS during the laser experiment. The burnt part is visible as a black spot on the PI. No signs of PDMS burning were observed. The top left contains PDMS and patterned CNTs. The square at the bottom left (square 1) indicates the PDMS/patterned CNT location during the experiment. No burning was observed on the PI sheet. Burnt sections were observed inside the PDMS, adjacent to the patterned CNT; (c–e) Top-view, bottom-view, and cross-sectional photographs of PDMS/patterned CNTs, respectively. Scale bars: 5 mm; (f) PDMS/patterned CNTs under 40% length compression; (g, h) Optical microscopy images of PDMS/patterned CNTs before and after laser irradiation, respectively; (i) Cross-sectional SEM image of PDMS-CNT after laser irradiation; (j, k) SEM images (top-view) of a burned area in the PDMS-CNT. Inset (j) EDS spectrum showing silicon oxide (SiOx) peaks in the burnt material.

magnitude increased on moving from a straight line to a pointed design. This pressure increase occurred owing to curvature, stress concentration, and a tendency to bend further in the direction of loading. The above behavior could be easily explained with help of a force balance, where a

large angle between the acting forces produced a better force distribution. In direction III, the stresses in the curved beam were smaller than those of the straight lines. This is because the beam tended to flatten by distributing the stresses towards the ends of the layers. The super-elastic behavior of the CNTs helped in this process. However, the sharp features of the pointed layer design dominated and hence produced a large stress peak.

We also demonstrated that the patterned CNTs in PDMS could be used in compressible laser shield applications. For this experiment, an infrared laser (1.06 μm) was focused over a polyimide (PI) sheet. A layer of PDMS containing patterned CNTs was placed over the sheet, between the PI and the laser (Figure 5a). A control experiment was performed under the same conditions using a pure PDMS layer with the same dimensions. Figure 5b shows the results of laser irradiation. Pure PDMS is transparent at the wavelength of the laser. Consequently, the laser burned the PI layer, as indicated by a black spot on the PI sheet. No signs of laser burning were observed if PDMS contained patterned CNTs. Instead, a grey, burned layer could be observed inside the PDMS. Figures 5c–e show the photographs taken after laser irradiation through patterned CNTs inside PDMS. The burned grey layer was located directly over the CNT layer, thus relating the laser absorption to the presence of the patterned CNT layer. The same laser shield effect was observed even under compression (Figure 5f). Optical microscopy images were taken before and after laser irradiation (Figure 5g, h respectively), which showed that the area between the CNT strips was also burned. The cross-sectional SEM image shown in Figure 5i correlates the burned area to the CNT strip position. The burned part was composed of a thin layer (<10 μm), over which CNT strips could still be observed (Figure 5j). Energy-dispersive X-ray spectrum (EDS) analysis of the layer identified the burned material as silicon oxide, which probably arose from the combustion of PDMS (inset, Figure 5j). High-resolution images demonstrated the presence of CNT bundles within the burned material. The reason that the laser did not penetrate the open spaces between the CNT strips is not clear; however, these composite structures can clearly be used both as optical switches and laser shields.

Conclusions

In conclusion, we demonstrate that the inherent anisotropic mechanical properties of CNTs can be used to fabricate a material with controllable optical transmittance, namely, the ability to transition from transparent to opaque at a strain of less than 0.4%. Lithography and CVD were used to design various (straight, corner-shaped, and curved stripes, as well as pillars) CNT forests in which optical switching depended heavily on the direction of loading. The transition was less pronounced when the samples were loaded in the longitudinal direction than in the perpendicular direction. Further, FEM analysis was used to illuminate the mechanical behaviors of the various CNT patterns. The CNT patterns were further demonstrated as both optical switches and structures for decreasing laser-induced damage.

Conflicts of interest

There are no conflicts to declare.

Acknowledgements

The authors thank the National Natural Science Foundation of China (Grant Nos. 51705247, 51435008, 51875577), the Air Force Office of Scientific Research (Grant FA9550-13-1-0084), the Air Force Office of Scientific Research MURI (Grant FA9550-12-1-0035), the China Postdoctoral Science Foundation (2017M611802) and Beijing Nova Program (No. Z171100001117058), for the financial support of the work presented. The authors acknowledge Yi Long from Nanyang Technological University (Singapore) and Souceng Tian, Mao Sheng from China University of Petroleum-Beijing for inspiring discussions on this paper.

Notes and references

1 M. Zhu, M. Zhu, J. Song, T. Li, A. Gong, Y. Wang, J. Dai, Y. Yao, W. Luo, D. Henderson and L. Hu, *Adv. Mater.*, 2016, **28**, 5181.
2 C.S. Tiwary, S. Kishore, S. Sarkar, D.R. Mahapatra, P.M. Ajayan and K. Chattopadhyay, *Sci. Adv.*, 2015, **1**,18.
3 P. Kim, Y. Hu, J. Alvarenga, M. Kolle, Z. Suo and J. Aizenberg, *Adv. Opt. Mater.*, 2013, **1**, 351.
4 F. López Jiménez, S. Kumar and P.M. Reis, *Adv. Opt. Mater.*, 2016, **4**, 620.
5 J. Xiang, Y. Li, Q. Li, D.A. Paterson, J.M.D. Storey, C.T. Imrie and O.D. Lavrentovich, *Adv. Mater.*, 2015, **27**, 3013.
6 A. Llordés, G. Garcia, J. Gazquez and D.J. Milliron, *Nature*, 2013, **500**, 323.
7 J. Zhou, Y. Gao, Z. Zhang, H. Luo, C. Cao, C. Zhang, L. Dai and X. Liu, *Sci. Rep.-UK*, 2013, **3**, 3029.
8 L. Long and H. Ye, *Sci. Rep.-UK*, 2014, **4**, 6427.
9 R. Baetens, B.P. Jelle and A. Gustavsen, *Sol. Energ. Mat. Sol. C.,* 2010, **94**, 87.
10 M.R. Shcherbakov, P.P. Vabishchevich, A.S. Shorokhov, K.E. Chong, D.Y. Choi, I. Staude, A.E. Miroshnichenko, D.N. Neshev, A.A. Fedyanin and Y.S. Kivshar, *Nano Lett.*, 2015, **15**, 6985.
11 A. Talin, E. Walter, A. Agrawal, T. Xu and H. Lezec, *Nano Lett.*, 2011, **11**, 2774.
12 T.Z. Shen, S.H. Hong and J.K. Song, *Nat. Mater.*, 2014, **13**, 394.
13 M. Dübner, V.J. Cadarso, T.N. Gevrek, A. Sanyal, N.D. Spencer and C. Padeste, *Acs Appl. Mater. Inter.*, 2017, **9**,9245.
14 X. Deng, L. Mammen, H.J. Butt and D. Vollmer, *Science*, 2012, **335**, 67.
15 A. Razmjou, M. Asadnia, O. Ghaebi, H.C. Yang, M.W. Ebrahimi, J. Hou and V. Chen, *ACS Appl. Mater. Inter.*, 2017, **9**, 38076.
16 Y. Ke, X. Wen, D. Zhao, R. Che, Q. Xiong and Y. Long, *ACS Nano*, 2017, **11**, 7542.

17 S. Magdassi, Y. Long, T.J. White, N. Wang, I. Abdulhalim, A.I.Y. Tok, I. Balin, Q. Lu and Y. Ke, *ACS Appl. Mater. Inter.*, 2016, **8**, 33112.
18 P.M. Ajayan, G. Brunetto, D.S. Galvão, S. Ozden, S.R. Bakshi, A. Roy, C.S. Tiwary and N.S. Karthiselva, *Adv. Mater. Interfaces*, 2016, **3**, 1500755.
19 P.M. Ajayan, R. Vajtai, T.N. Narayanan, A.H.C. Hart, S. Ozden, C.S. Tiwary, C.S. Tiwary and P. Dong, *Small*, 2015, **11**, 688.
20 P.M. Ajayan, A.C. Chipara, R. Vajtai, R. Romero-Aburto, J. Taha-Tijerina, A.H.C. Hart, S. Ozden, C.S. Tiwary and M.T.F. Rodrigues, *Adv. Mater.*, 2015, **27**, 1842.
21 P.M. Ajayan, R. Vajtai, A.C. Hart, J. Lou, E.V. Barrera, C.S. Tiwary, P.S. Owuor, R. Koizumi and M. Soto, *Adv. Eng. Mater.*, 2017, **19**, 1600756.
22 P.M. Ajayan, R. Vajtai, C.F. Woellner, D.S. Galvão, S. Ozden, J. Lou, J.M. Tour, B. Wei, T. Li, S. Vinod, C.S. Tiwary, S. Kosolwattana, P.S. Owuor, S. Bhowmick and L.X. Duyet al., *Adv. Mater. Interfaces*, 2017, **4**, 1700030.
23 S.K. Jeoung, N. Jalili, R. Ghosh, Y.J. Jung, A. Vaziri, P. Su, S. Hong, J. Hao, T. Lundstrom, J. Suhr and H. Abdi, *ACS Appl. Mater. Inter.*, 2016, **8**, 34067.
24 S. Esconjauregui, S. Hofmann, B. Chen, G. Zhong, J. Robertson, C. Zhang, H. Tornatzky and P.G. Oppenheimer, *ACS Appl. Mater. Inter.*, 2015, **7**, 3626.
25 P.M. Ajayan, J.A. Bur, L. Ci, Z. Yang and S. Lin, *Nano Lett.*, 2008, **8**, 446.
26 H. Kishida, Y. Hayamizu, K. Hata, K. Mizuno, M. Yumura, S. Yasuda, D.N. Futaba and J. Ishii, *P. Natl. Acad. Sci. Usa.*, 2009, **106**, 6044.
27 M.N. Ghasemi-Nejhad, P.M. Ajayan, A. Cao, W.G. Sawyer and P.L. Dickrell, *Science*, 2005, **310**, 1307.
28 Z. Tang, Z. Tang, Q. Gan, A. Cao, Z. Lin, Z. Zeng, H. Li, Y. Zhu, R. Xiang and X. Gui, *Adv. Mater.*, 2014, **26**, 1248.
29 P.M. Ajayan, P.K. Patra, G.G. Silva, L. Ci and B.J. Carey, *ACS Nano*, 2011, **5**, 2715.
30 C. Sow, J.T. Thong, T. Yu, W. Ji, H.I. Elim, Y. Zhu, Z. Shen, J. Lee, A.T. Wee, Y. Foo and Y. Liu, *Adv. Mater.*, 2006, **18**, 587.
31 S. Yang, E. Lee, Y. Cho, D.S. Gianola, M. Li, L. Yang and D. Ge, *Adv. Mater.*, 2015, **27**, 2489.
32 J. Natoli, L. Gallais, H. Akhouayri and C. Amra, *Appl. Optics*, 2002, **41**, 3156.
33 C.B. Schaffer, A. Brodeur and E. Mazur, *Meas. Sci. Technol.*, 2001, **12**, 1784.
34 M.D. Perry and G. Mourou, *Science*, 1994, **264**, 917.
35 D.O. Vidaud, A.J. Hart, S.J. Park, S.H. Tawfick, M.F.L. De Volder, M.F.L. De Volder and M.F.L. De Volder, *J. Micromech. Microeng.*, 2011, **21**, 45033.
36 C. Liu, H. Ding, Z. Wu, B. Gao, F. Fu, L. Shang, Z. Gu and Y. Zhao, *Adv. Funct. Mater.*, 2016, **26**, 7937.
37 Z. Yang, L. Ci, J.A. Bur, S. Lin and P.M. Ajayan, *Nano Lett.*, 2008, **8**, 446.
38 K. Mizuno, J. Ishii, H. Kishida, Y. Hayamizu, S. Yasuda, D.N. Futaba, M. Yumura and K. Hata, *P. Natl. Acad. Sci. Usa.*, 2009, **106**, 6044.
39 M.N. Ghasemi-Nejhad, P.M. Ajayan, C. Soldano, A. Cao, A. Cao, S. Kar, S. Kar, X. Li, X. Li, V.P. Veedu, K. Ma and K. Ma, *Nat. Mater.*, 2006, **5**, 457.

Table of Contents

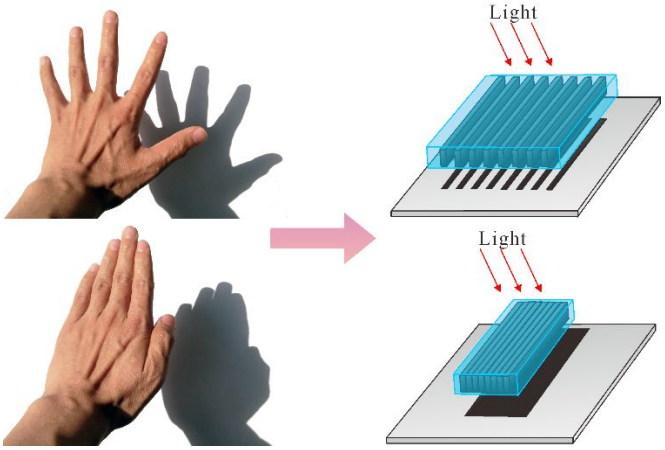

This work develops a CNT/PDMS composite structure with tunable optical transmittance in response to a strain of less than 0.4%.